Bull. Chem. Soc. Ethiop. **2025**, 39(4), 763-780.
DOI: https://dx.doi.org/10.4314/bcse.v39i4.12

ISSN 1011-3924
Printed in Ethiopia
Online ISSN 1726-801X

COMPREHENSIVE ANALYSIS OF INDOLE-2-CARBOXYLIC ACID AS AN ANTIOXIDANT DRUG: SPECTROSCOPIC, QUANTUM CHEMICAL, TOPOLOGICAL AND MOLECULAR DOCKING STUDIES

V.S. Jeba Reeda[1], J.N. Cheerlin Mishma[1], P. Divyab, Nazrul Haq[3], S. Muthu[4], Nazia Siddiqui[5] and Saleem Javed[6*]

[1]Department of Physics, Easwari Engineering College, Ramapuram, Chennai 600 089, Tamil Nadu, India
[2]Department of Physics, Saveetha School of Engineering, Saveetha Institute of Medical and Technical Sciences (SIMATS), Thandalam, Chennai 602 105, Tamil Nadu, India
[3]Department of Pharmaceutics, College of Pharmacy, King Saud University, Riyadh 11451, Saudi Arabia
[4]Department of Physics, Aringnar Anna Govt. Arts College, Cheyyar-604407, India
[5]Department of Chemistry, Dayalbagh Educational Institute, Agra, 282005, U.P., India
[6]Department of Chemistry, Jamia Millia Islamia, New Delhi, Delhi 110025, India

(Received September 4, 2024; Revised December 16, 2024; Accepted December 18, 2024)

ABSTRACT. Bioactive indole-derived compounds have become increasingly important in current years owing to their wide range of biological and pharmacological uses. In this work, vibrational, electrical, physicochemical, and suppressive attributes of Indole-2-carboxylic acid (ID2CA) are predicted and analyzed. First, the molecular structure of ID2CA was refined, and its structural characteristics were computed in different environments, including polar solvents (DMSO, methanol, and water) as well as in the gas phase. A strong correlation was observed between the molecule's simulated and experimentally obtained infrared spectra. Measured UV-Visible spectra confirm the ID2CA's $\pi \rightarrow \pi^*$ electronic shift, which is compatible with the computed spectra. Subsequent examination of FMO revealed intramolecular charge transfer (CT) throughout the molecule, highlighting ID2CA's bioactivity. To verify findings of the natural charge assessment and FMOs, Fukui function values were computed. ID2CA was discovered to be a significant part of the antioxidant resistance system by molecular docking studies. After performing 100 ns MD simulations and effective free energy computations with MMPBSA, durability of the best-docked protein (2C9V) was evaluated.

KEY WORDS: Fukui function, MMPBSA, Molecular dynamics simulations

INTRODUCTION

Indole, a planar bicyclic heterocyclic structure, is prevalent in a wide range of medically significant compounds [1]. It is made up of a five-membered pyrrole ring that contains nitrogen linked to a six-membered benzene ring. Indole, based on Huckel's rule, "is an aromatic framework containing a total of 10 π-electrons, 8π from double bonds, and 2π from the nitrogen atom" [2]. Owing to π electrons' delocalization, electrophilic replacement processes can be readily facilitated. Moreover, pyrrole ring of indole contains a somewhat acidic N-H bond, which enables N-substitution processes to occur in basic conditions [3]. Indole's capability to mimic molecular makeup of peptides and interact reversibly with enzymes makes it extremely beneficial in drug discovery [4]. Several indole derivatives have a variety of pharmacological characteristics, such as immunomodulatory, antioxidant, antitubercular, antiulcer, antimalarial, antibacterial, antiplatelet, and antileishmanial effects. These features have resulted in substantial research into indole chemistry and chemical synthesis [5]. For instance, while Kalaskar and co-workers [6]

*Corresponding authors. E-mail: saleem.7javed@gmail.com, dr.naazsiddiqui@gmail.com

produced indole-3-acetic acids and examined there anti-inflammatory efficiency, Rani *et al.* [7] examined the "anti-inflammatory characteristics of heterocyclic indole derivatives". Meenakumari *et al.* [8] discovered that methyl indole-3-carboxylate hinders the action of "mitogen-activated protein kinase 14", a protein associated with cervical cancer, implying the possibility for novel cervical tumour treatments. Hany [9] conducted a study on the preparation, characterization, in vitro biological evaluation, DFT calculations, and molecular docking of 1H-imidazole-2-carboxylic acid. The findings demonstrated its strong binding interactions with target proteins, emphasizing its potential for therapeutic applications.

Despite comprehensive research searches and forecasts, not one investigation on indole-2-carboxylic acid's structural, electrical, and antioxidant characteristics has been uncovered. Consequently, the goal of this work is to examine its molecular and spectral properties by using DFT as a potent tool. Computational investigations have been conducted to evaluate geometric characteristics, optimum energy, FMO, and MEP for gas and polar solvents (DMSO, methanol, and water) via DFT/IEFPCM/B3LYP/6-311++G(d,p) basis set. Topological assessments, including LOL, RDG, and ELF, done with a multi-wave function program, are utilized to understand the energy density of electrons. Furthermore, distinct parts will cover ID2CA's thermodynamic variables, nonlinear optical features, Fukui functions, and charge analysis. Measuring drug-likeness projections is employed for assessing possible drugs from different sources, and molecular docking assays were utilized to uncover probable binding pathways of ID2CA with target proteins, clarifying its antioxidant function. After running 100 ns of molecular dynamic simulations, durability and energies were examined using MMPBSA computations.

EXPERIMENTAL

FT-IR spectra in solid state of ID2CA were acquired in 4000-600 cm^{-1} span with a PerkinElmer Spectrum, with a KBr beam splitter. A UV-1280 Multipurpose tool (spectrophotometer) was exploited in ultraviolet (200–800 nm) range for the UV investigation in DMSO and methanol as the solution form.

Computational facts

DFT simulation was undertaken for ID2CA utilizing Gaussian'09 program [10] package, leveraging B3LYP/6-311++G(d,p)[11] for gas and polar liquids. The ID2CA molecule's vibrational allocations were identified utilizing NCA with Sundius' MOLVIB [12] version 7.0. GaussSum [13] and GaussView 5.0 [14] software were used to visualize the results of UV-Vis, FMO, and MEP investigations that were conducted in a variety of solvents, such as DMSO, methanol, and water. Multiwfn [15], a multifunctional wave function modeling tool, was utilized to examine RDG, LOL, ELF, electron-hole evaluation, and isosurface graphs, which were portrayed with VMD software [16]. The target compound's drug-likeness was evaluated therapeutically using the SwissADME [17]. Docking investigations were carried out with AutoDock version4.2.1 [18], and visualized via Discovery Studio [19]. Molecular dynamics [20] modeling was implemented to investigate macromolecule elasticity and the effect of movement on drug-ligand interactions, employing the GROMACS 5.1 [21] tool for predicting ligand-enzyme mixtures and the Swiss Param [22] web-based tool for assessing ligand characteristics.

RESULTS AND DISCUSSION

Structural Conformation

The DFT simulation used [aforesaid basis set] to uncover the best structural configuration by integrating bond length (BL) and angle (BA). Figure 1 depicts the optimal arrangement of atomic

molecules and Table 1 contains a list of parameters of geometry for both gas and solvents phase. Since there are currently no experimental info available for the molecule ID2CA, the XRD data of CCDC 216179 [23] compound was compared to speculated computation BL, BA, and DA. The remainder of the predicted values, with the exception of a few optimized morphological characteristics, agree with the experiment's findings. Linear regression investigation was employed to evaluate the coefficients of linear correlation (R2) for likening conceptual and experimental BL and BA. The BL RMSD values were discovered to be 0.98355 (gas), 0.98465 (DMSO), 0.98464 (methanol), and 0.98467 (water), while the BA RMSD values were 0.95827 (gas), 0.96357 (DMSO), 0.96349 (methanol), and 0.96365 (water). There is an excellent level of concordance among both hypothetical and experimental frameworks, as indicated by these minimal coefficient values. Though experimental calculations were done in the solid state and were impacted by intermolecular relations with crystallographic arranging effects, the hypothetical computing conducted in the gaseous phase are responsible for the slight discrepancy that exists between hypothesized and observed parameters.

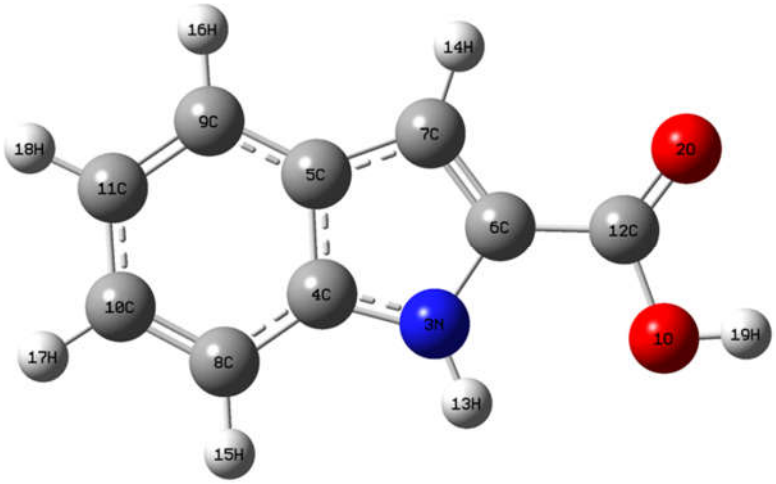

Figure 1. Optimized structure of ID2CA molecule for gas phase.

In the present study, ID2CA has 9 (C-C), 5(C-H), 2 (O-C), 2 N-C, one (N-H). CCH and NCC angles have been noticed and confirmed to be 119-128° and 109-122°, respectively, with OC bond lengths lying around 1.367 Å. The length of the NC bond was determined to be 1.37-1.38 Å, while the angles of the OCO and COH were calculated to be 111° to 125°, and 107°, respectively. CCC angles were discovered to be between 106° - 133°, while C-C BL ranged from 1.376 to 1.460 Å. The predicted lengths of the CH bonds were found to be between 1.072 and 1.084 Å, whereas the anticipated CCH angles were 109-122°, respectively. BL C_9-H_{14} (1.0784 Å) is petite than experimental value bond length (0.9317 Å), suggesting the existence of double bond features in O_2-C_{12} bond. All C-C bonds in indole ring have lengths between 1.37 Å and 1.46 Å, which match the value found in the experiment. Because there is an electronegative oxygen atom present, the O_1-H_{19}, O-C BL is shorter than other C-C bonding values. When developing molecules with exceptional biological products profiles, it is imperative to consider that intramolecular N_3-H_{13}···O_1 and C_7-H_{14}···O_2 hydrogen bonding interactions occur with N-H···O, C-H···O values of 2.72 and 2.94, respectively, and these values are significantly fewer than the vdW leaving (<3) between each O and H atom [24]. The highest bond length that was 1.4602 Å between C_6-C_{12}

atoms. Moreover, O_1-H_{19} has a lower BL (0.9682). Overall, the length of a ring's bonding (C-C) spans from 1.376 to 1.460 Å for gas, 1.3797 to 1.46 Å for DMSO, 1.379 to 1.46 Å for methanol and 1.379 to 1.46 Å for water. The bond of separation between C and C atoms (C_6-C_7), are 1.376 (gas), 1.374 (DMSO), 1.37097 (methanol) and 1.379 (water). DFT approach calculates the SCF [25] energy to be -552.554 Hatrees. For solvent DMSO = water = methanol = -552.560 Hatrees all these solvents show similar SCF. Excellent concordance is shown between the computed C_8-C_{10}-C_{11} bond angle of 121.548° and the experimental (XRD) value of 121.51° also for O_2-C_{12}-C_6 bond angle is 125.9° and experimental matches approximately which is equal to 125.8°. It is possible to conclude that there exists an adequate agreement among the experimental and theoretical geometrical variables in light of the aforementioned observations. Additionally, the computed bond lengths in ID2CA molecule exhibit an important connection with almost structurally comparable molecules found in the literature. Based on these findings, we can determine if the gas phase is less dependable than the solvent. We may safely infer that this strategy enhanced the tangible parameters of the selected structural-model. There is little difference between gas and polar solvents.

Table 1. Optimized bond length of ID2CA for gas phases and solvents.

Bond length	Gas	DMSO	Methanol	Water	Experimental
O_1-C_{12}	1.3674	1.3545	1.3547	1.3543	1.3257
O_1-H_{19}	0.9682	0.9697	0.9697	0.9698	0.9512
O_2-C_{12}	1.2079	1.2151	1.215	1.2152	1.2272
N_3-C_4	1.3717	1.3703	1.3703	1.3702	1.3827
N_3-C_6	1.3872	1.3858	1.3859	1.3858	1.3841
N_3-H_{13}	1.0072	1.0086	1.0086	1.0086	0.9692
C_4-C_5	1.4253	1.4263	1.4263	1.4263	1.4034
C_4-C_8	1.4003	1.4018	1.4018	1.4019	1.3903
C_5-C_7	1.4263	1.4256	1.4256	1.4256	1.4165
C_5-C_9	1.4081	1.4098	1.4098	1.4098	1.4093
C_6-C_7	1.3769	1.3797	1.3797	1.3798	1.3693
C_6-C_{12}	1.4602	1.46	1.46	1.46	1.4392
C_7-H_{14}	1.0784	1.0785	1.0785	1.0785	0.9317
C_8-C_{10}	1.3848	1.3851	1.3851	1.3852	1.3723
C_8-H_{15}	1.0841	1.0836	1.0836	1.0836	1.046
C_9-C_{11}	1.3826	1.3832	1.3832	1.3832	1.3573
C_9-H_{16}	1.0842	1.0842	1.0842	1.0842	0.9747
C_{10}-C_{11}	1.4131	1.4153	1.4152	1.4153	1.4034
C_{10}-H_{17}	1.084	1.0841	1.0841	1.0841	1.0272
C_{11}-H_{18}	1.0838	1.0839	1.0839	1.0839	0.9647
RMSD	0.98355	0.98465	0.98464	0.98467	

NBO analysis

The exploration of natural bonding orbitals, or NBOs, provides valuable details concerning the conjugation and hyperconjugation of molecular networks as well as logical conceptual knowledge concerning intra- and ICT [25]. NBO was performed with a TD-DFT/B3LYP 6-311++G(d,p) basis set. The number of electrons in atomic structures was measured using the NBO approach, which also evaluated the relationship among Lewis-type givers and non-Lewis receiver NBOs. Balanced basis sets increase exactness and effectiveness in the understanding of intra- and between molecules connection, conjugation, hyper-conjugation, and CT in molecules. The change energies associated with donor-acceptor connections are displayed in Table S2 for the ID2CA compound. $\pi(C_6–C_7) \rightarrow \pi^*(O_2–C_{12})$, $\pi(C_4–C_5) \rightarrow \pi^*(C_6–C_7)$ have 22.96 and 20.59 kcal/mol, $\pi(C_9–C_{11}) \rightarrow \pi^*$ $(C_8–C_{10})$ and $\pi^*(C_9–C_{11})$ has 16.84 and 18.81 kcal/mol, $\pi(C_8–C_{10}) \rightarrow$

$\pi^*(C_9–C_{11})$ and $\pi(C_9–C_{11}) \rightarrow \pi^*(C_4–C_5)$ have 16.35 and 16.3 kcal/mol and $\pi(N_3–H_{13}) \rightarrow \pi^*(C_4–C_5)$ have 1.84 kcal/mol. These perturbation energies provide the compound with stronger stabilization. Table clearly shows that the intramolecular "hyperconjugation interaction of the σ and π electrons of C-C and N-H to the anti-(C-C and C-N) bonds in the ring" is accountable for stabilization of certain portions of ring. Stabilization energy of all these transitions correspond to only four pairs of orbitals: C_4-C_5, C_9-C_{11}, C_6-C_7 and N_3-H_{13}. Consequently, the findings imply that the π nature of the hybrid orbitals controls these orbitals. A molecule's Lewis structure is regarded as acceptable if all orbitals in the formal Lewis structure have an occupancy greater than a particular threshold, which is typically between 0.29 and 0.59 electrons. Based on electron-donating from $LP(2)O_1 \rightarrow \pi^*(O_2–C_{12})$ and $LP(1)N_3 \rightarrow \pi^*(C_4–C_5)$, which exhibit a greatest stabilisation of 39.39 and 37.75 kcal/mol, the binding energy of resonance in the compound is calculated. Key interactions are $LP(2)O1 \rightarrow \pi^* (O_2–C_{12})$ which has the uppermost E(2) of 39.39 kcal/mol in gas and 43.43 kcal/mol (DMSO), 43.36 kcal/mol (methanol) and 43.5 kcal/mol (water), regarding a tiny change from the preceding sequence: DMSO $\pi^* (O_2–C_{12}) \rightarrow \pi^*(C_6–C_7)$ (91.79 kcal/mol), methanol $\pi^* (O_2–C_{12}) \rightarrow \pi^* (C_6–C_7$ kcal/mol) (91.5 kcal/mol), water $\pi^*(O_2–C_{12}) \rightarrow \pi^*(C_6–C_7)$ (91.69 kcal/mol). Solvent effect in ID2CA compound plays important role and it significantly affects the interaction. This is a very good result because Table 2 clearly shows that the solvents and gas phases were comparable and that the title compound was significantly affected by solvent impacts. The compound's remarkable medicinal potential may instigate from largest contact occurring in the ring.

Vibrational analysis

The comprehension of bonding energies and the potency of both intramolecular and intermolecular connections is largely dependent on vibrational analysis. Vibrational spectroscopy and quantum computations together provide important new information about the vibrational assessment of bioactive substances. Examining structural form and identifying functional categories in organic compounds are made possible by this method. After assigning vibrational bands using the NCA approach, SQMFF computations are utilized to fine-tune the frequencies. The ID2CA molecule, which consists of 19 atoms, has 51 normal vibrations. The measured and theoretically predicted FT-IR spectra are exposed in Figure 2.

COOH vibrations

Carboxylic acid vibrational analysis is predominantly based on carbonyl and hydroxyl groups. The carbonyl and hydroxyl groups of carboxylic acid are the main basis for vibrational analysis. Strong absorption appears to occur in the [26] 3700-3400 cm^{-1} area for the isolated hydroxyl group. Hydrogen-bonded species' FT-IR spectra show clear shifts in O-H vibrations, which are tremendously sensitive to their surroundings. Wide and medium to strongly intense, the band in infrared spectrum is ascribed to νS(O-H). In FTIR spectra of ID2CA with 100% PED, the νS(O-H) vibration of the carboxylic acid group seems as a prominent band at 3463 cm^{-1}. β(O-H) bands are generally easier to distinguish from C-H bending bands because they are usually wider, falling between 1440 and 1395 cm^{-1}. The O-H group is capable of bending in and out of the plane outlined by the acid component. The β(O-H) vibrations are associated with peak at 1399 (w) cm^{-1} (FT-IR), which correlate to a scaled value at 1392 cm^{-1} with 43% PED.

When it comes to relatively little changes in its surroundings, the carbonyl (C=O) group is highly sensitive and shows a significant amount of absorbance in the FT-IR spectrum. A variety of intra- and intermolecular factors influence carbonyl absorptions; prevalent organic substances exhibit impacts related to conjugation, mesomeric, inductive, and field. Acids have far more significant νS(C=O) bands than ketone C=O stretch bands. Usually, νS(C=O) vibration of -COOH can be noticed in the range of [27] 1750–1650 cm^{-1}. ID2CA exhibits a faint νS(C=O) vibration at

1777 (vw) cm^{-1} in FT-IR, which is blue-shifted by approximately 27 cm^{-1} owing to intramolecular C_7-H_{14}···O_2 H-bonding interactions. The νS(C-O) vibration, which emerges in the [28] 1260-1000 cm^{-1} range, is a distinctive band that depends on branching. As the molecule's replacement and conjugation upsurges, νS(C-O) band changes to decrease frequencies. The estimated νS(C-O) in ID2CA is detected at 1300 cm^{-1}, somewhat blue-shifted owing to intramolecular N3-H13...O1 H-bonding interactions, and is in precise accord with the experimentally measured value of 1308 cm^{-1}.

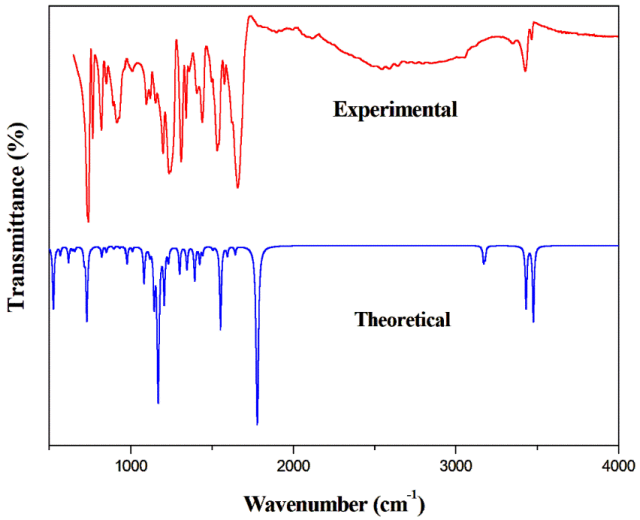

Figure 2. Experimental and simulated FT-IR spectra.

NH vibrations

νS(N-H) produces distinct vibrational bands, which are easy to distinguish. Generally, the νS(N-H) wavenumber is observed to be more than 3200 cm^{-1} [29]. νS(N-H) mode is responsible for a very robust band that appears at 3419 cm^{-1} (FT-IR). The computed νS(N-H) has a high PED of 99% and emerges at 3430 cm^{-1}. β(N-H) vibrational states are delineated at smaller frequencies, notably about 1641 to 1085 cm^{-1}. In FT-IR, a combination of vibrations is apparent at 1195 (vs) cm^{-1} owing to νS(C-C) and νS (C-N) bond with 52% PED contributions.

CH vibrations

The distinctive range of 3200-3000 cm^{-1} is where νS(C-H) vibrations in heteroaromatic moieties, such as indole, are usually detected. Here, the substituent's nature has no discernible effect on the bands [30]. The five predicted C-H vibrations of stretching match the stretching modes of C_7-H_{14}, C_9-H_{16}, C_{11}-H_{18}, C_{10}-H_{17}, and C_8-H_{15} units, respectively. In ID2CA, νS(C-H) vibrations are ascribed to the FT-IR bands detected at 3343 (vw), 3121 (vw), and 3057 (vw) cm^{-1}. The specified basis set at 3243-3155 cm^{-1} predicts scaled vibrations (mode nos. 3–7) that exhibit excellent agreement with the spectral data that was observed. In light of intramolecular C_7-H_{14}···O_2 H-bonding interactions, the wave number 3343 for (C_7-H_{14}) predicts a blue shift. Aromatic β(C-H) in-plane vibrations occur between [31] 1300-1000 cm^{-1}. Although bands are crisp, their intensity is modest to medium. Outstanding concordance is seen between the β(C-H) in-plane vibrations estimated at 1231, 1143, 1116, and 1081 $cm^{-1}$and FT-IR bands at 1229 (vs), 1147 (w),

1116 (w), and 1091 (w) cm^{-1}. FT-IR bands at 921 (vs), 853 (w), 823 (vs), and 734 (vs) cm^{-1} correspond to ω(C-H) out-of-plane vibrations in ID2CA. This aligns well with hypothetically scaled harmonic wavenumber values at 934, 852, 823, and 733 cm^{-1} (mode nos. 28, 30, and 31) using the B3LYP approach.

CC and CN vibrations

Generally, in aromatic hetero molecules, νS(C-C) vibrations are detected in [32] 1400-1650 cm^{-1} range. In ID2CA, FT-IR observations of νS(C-C) vibrations at 1655 (vs), 1576 (s), and 1530 (vs) cm^{-1} are in fairly good accord with scaled values. Instead of determining the kind of replacement, the shape of the swapping around the ring determines the precise placements. The estimated range of ring νS(C=C) vibrations is 1300-1000 cm^{-1}, but the FT-IR observation of a feeble band at 1357 cm^{-1} agrees with scaled value of 63% PED. vs(C-N) ascend in the area of [33]1200–1400 cm^{-1} in strong extent and are frequently mixed with extra bands, particularly C–C and βCH bands.

UV spectral analysis

For purposes of use, non-linear optical materials need to have transmission bands. With aforesaid basis set, (TD) DFT approach was exploited to conceptually determine the electron' UV–Vis transitions. Take into consideration the fact (TD-DFT), which offers the optimal interfere with reliability and computational expenses, has lately become a potent utensil for exploratory both the stationary and dynamic features of compounds when in their states of excitation [34]. The computations are performed in a variety of solvents, including DMSO, methanol and Water along with in gas. In experiments, DMSO and methanol solvents are utilized. With the use of the GaussSum programme [13], the transitions' primary contributions were identified. The visual peak absorption values of this molecular structure, according to estimations of the orbiting geometry, correlate to the proton shift through FMO, such as interpretation across “HOMO to LUMO, HOMO-1 to LUMO, and from HOMO to LUMO+1”. The computed absorbance peak detected at 280.77 (gas phase), 289.14 (DMSO), 287.54 (methanol), and 287.63 (water). The results of the experiment were perfectly consistent with theoretically estimated values. The maximum absorption value is shown at 293 nm (DMSO) and 292 (methanol) in this experimental observation band. Computed and observed wavelengths in gas and other solvents are almost equal, suggesting that the solvent may have an impact on the optical characteristics of the molecule. The strong transition seen in the gas phase at 280.77 nm is associated with an oscillator strength of f = 0.3816, corresponding to an energy gap of 4.416 eV. However, in the case of ID2CA solvents, there is a persistent shift characterized by a significant increase in oscillator strength within the solvent-based solution. The computed absorption maximum values in this subsequent instance are 287.63 (water), 287.54 (methanol) and 289.14 nm (DMSO), respectively, with an oscillator strength of f = 0.4871, 0.4861 and 0.5167. The intensive electronic shift predictions are of the π-π* form. Since the enhanced smell within the thiophene ring was predicted to cause the π-π* transitions to be seen effectively at lower wavelengths that are the change in wavelength virtually corresponds to π-π* bands.

FMO study

For quantum biology, those with the most significant (FMOs), such as the (LUMO) and the (HOMO), are crucial variables. They are essential to the molecule's chemical equilibrium [35]. They are frequently denoted to as the FMO because they allow us to able to ascertain how the molecules interfaces alongside other species of matter. In this assignment, the density of the state (DOS) has been generated by using the GaussSum programme [13] to figure out the contributions of groups to the molecular orbitals. The DOS plot provides a basic understanding of the

characteristics of the orbitals of molecules within a specific energy spectrum by displaying the analysis of populations per orbital structure. The chemical's electrical characteristics are derived via its DOS band. Energy gap value reported by DOS corresponds to the wavelength discrepancy values revealed by UV-Vis and atomic orbital investigations. For gas phase, HOMO-LUMO changes occurred at -6.258 and -1.840 eV, respectively. The DOS diagram depicts the molecule's HOMO-LUMO transition. According to DOS studies, the electron cloud may be utilized for enabling the e-transport capability. As a result, it is clear that the solvent widens the spectral gap.

Table 2. Calculated energy values of title compound by B3LYP /6-311++G(d, p) for gas and solvents.

Parameters	Gas	DMSO	Methanol	Water
HOMO (eV)	-6.258	-6.289	-6.288	-6.286
LUMO (eV)	-1.840	-1.927	-1.920	-1.986
Ionization potential	6.258	6.289	6.288	6.286
Electron affinity	1.840	1.927	1.920	1.986
Energy gap (eV)	4.418	4.362	4.368	4.300
Electronegativity	4.049	4.108	4.104	4.136
Chemical potential	-4.049	-4.108	-4.104	-4.136
Chemical hardness	2.209	2.181	2.184	2.150
Chemical softness	0.226	0.229	0.229	0.233
Electrophilicity index	3.711	3.869	.856	3.978
electronic charge	1.833	1.884	1.879	1.924
electron donating capability (w-)	6.011	6.195	6.181	6.315
electron accepting capability (w+)	1.962	2.087	2.077	2.179
Dipole moment	3.1099	4.1591	4.1948	4.1775

When it comes to electron contributions, the HOMO orbital is typically employed, while the LUMO orbital is primarily used as an electron receiver. Molecular chemical resistance is defined as the difference among HOMO and LUMO. The frontier orbital gap provides information about the molecule's kinetic endurance and chemical reactive properties. We have performed computations in gas and numerous additional solvents, including DMSO, methanol and water in order to accurately assess the physical behaviour of the chemical under investigation. TD-B3LYP technique predicts both and the findings show that there are 42 occupied orbitals of molecules and 269 vacant virtual molecular orbitals in the molecule. The patterns of distribution and quantities of energy of FMO orbitals during the gas state for the ID2CA compound are displayed in Figure3. Red denotes positive layer while green denotes the negative portion. Figure 3 makes it evident that the ring and the isodensity graphs associated with HOMO are well-localized. In overall, a particle has a higher density of HOMO occupancy ought to be better in its capacity to extract a proton, while an atom with a higher density of LUMO occupancy ought to be capable to receive an electron. At 1.600 eV, the LUMO orbital components are of the π-π^* type. Consequently, an extremely narrow energy gap of 4.418 eV is computed among the HOMO and LUMO orbitals of molecules. The material under study exhibits a remarkable huge energy gap (Eg = 4.362 eV) between its outermost orbitals. This value is somewhat smaller than that of water, with an energy gap of 4.300 eV, and comparable to that of methanol & DMSO, both of which possess an Eg = 4.368 eV. Therefore, ID2CA the chance of an electron transfer from the HOMO and LUMO orbitals is highly probable (π-π^*). In the case of ID2CA, the frontier orbital gaps are smaller, resulting in it less resilient and more responsive. A molecule known as a "soft molecule" has a tiny frontier orbital gap, which makes it susceptible to polarisation and typically related to high chemical reactive properties and low dynamical stabilisation. Apart from the energy discrepancy, a substance's chemical durability can also be inferred from its chemical toughness and brittleness, and its moment of dipole is a crucial electrical characteristic. For instance, the interactions between molecules will be greater the larger the dipole moment. From Table 2, it becomes

apparent how the dipole moment's value rises as one move through the gas state (3.1099 D) towards the solvent shift (3.137 D in DMSO), based on expected dipole moment values.

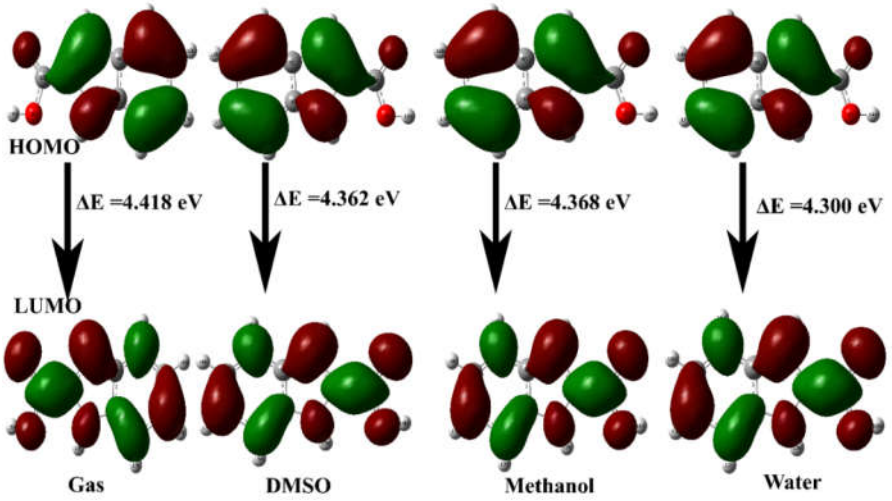

Figure 3. Frontier molecular orbitals of ID2CA molecule with different solvents.

MEP analysis

In order to investigate bonds of hydrogen associations and bio-recognition infrastructure, the MEP, is an essential property for assessing the location of activity of electrophilic and nucleophilic impacts on a molecular structure [36]. The calculated MEP for gas and solvent phases (DMSO, methanol and water). For electrostatic-potentials on each atom MEP fields have been represented by colour coding that has been mapped within the range of -6.470 e^{-2} to 6.470 e^{-2} (gas phase). Color codes fall between -7.357 e^{-2} to 7.357e^{-2} (DMSO), -7.341 e^{-2} to 7.341 e^{-2} (methanol), 7.372 e^{-2} to 7.372 e^{-2} (water). In MEP, "red denotes the presence of electrons with a low electrostatic charge potential, green denotes intermediate energy potential", and blue denotes a shortage of electrons due to a high electrostatic potential [37].

The largest number of positively charged spots are found in the N-H areas, whereas the electrostatic attraction of the oxygen atom is negative. Consequently, the H···O region is susceptible to electrophilic threat, whereas the N-H region is susceptible to nucleophilic interference. In terms of adapting atomic charge to electrostatic potential, O_1 and O_2 (-0.65 e and -0.582 e) were among the most electronegative atoms in gas. For these electrophilic sites, the electrostatic charge value for O_1 and O_2 be the greatest negative site. Calculated point charges which is roughly (0.752 a.u.), are shown to be significant amid others. Amongst those with the greatest positive charged atoms in gas were C_{12} and H_{19} (0.752 e and 0.4372). Over the MEP exterior, the region surrounding N_3 and however, appears blue since the majority of electron surrounds N atoms of ID2CA. Furthermore, it has been found that the ring carbon atoms has significant positive charges. The electro-negative difference inside the molecule is shown to be negligible, based on the MEP investigation of ID2CA. This finding is explained by the existence of many charges dispersed throughout the intermediary potential location, especially around the ring. The acquisition of reacting areas inside the substance, which is aided by interactions between electrons and protons, provides more evidence for the biological effects of ID2CA.

Fukui function (FF)

The Fukui function, often used to forecast reactive sites, is a key idea in DFT theory [38]. Using the FF and dual descriptor (Δf(r)), electrophilic assault locations for the ID2CA molecule were examined to understand chemical reactivity better. The dual classifiers and Fukui functions for every atomic site were thoroughly investigated. Fukui functions and dual classifiers for gas phase are shown graphically at a 0.005 isovalue in Figure 4, with blue regions indicating negative places vulnerable to electrophilic assault and green areas signifying positive locales.

Morrell *et al.* [39] also created a useful technique called the dual descriptor for detecting reactive areas. In formal terms, there is a close relationship involving the FF and Δf(r), which is written as "$\Delta f(r) = f^{+}(r) - f\text{-}(r)$". Unlike the Fukui function, f allows both kinds of locations that react to be accessible at the same time. If $\Delta f(r) > 0$, then the location is beneficial for an electrophilic assault; if $\Delta f(r) < 0$, then it is excellent for a nucleophilic assault. The dual descriptor function demonstrated that the electrophilic properties of atomic locations are N_3, C_8, C_9, C_7, C_6, C_{11}, and C_5 (in gas phase) and N_3, C_8, C_9, C_{11}, C_7, C_{10}, C_6, and C_5 (in solvents). Atomic locations C_{12}, O_2, O_1, C_4, C_{10} (in the gas phase) and C_{12}, O_2, O_1, C_4 (in solvents) are further characterized as having a nucleophilic assault nature. Significantly, it was shown that oxygen atoms bound to carbon atoms show strong nucleophilic characteristics.

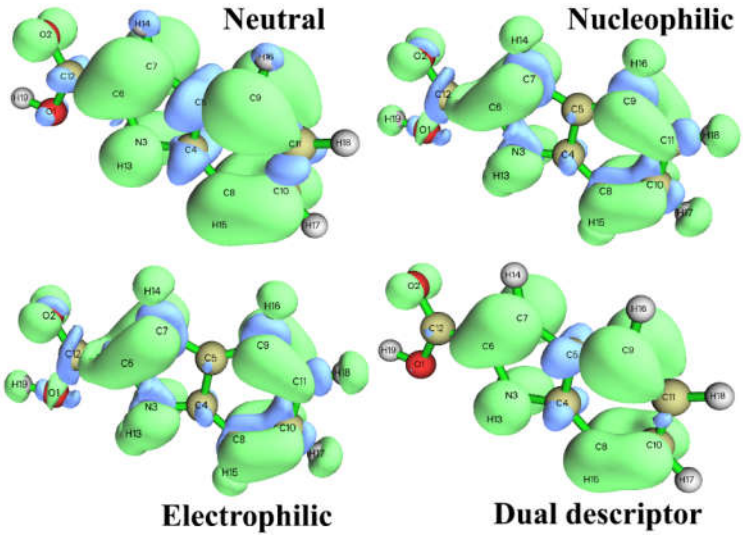

Figure 4. Fukui functions and dual descriptor for ID2CA in gas phase.

Natural charge examination

Natural charge study is a superior method to examine distribution of charges of ID2CA since it does not show basis set dependency. Plotted in table, the atomic charges are computed by natural charge analysis. Accumulation of charge over oxygen's electronegative side atoms, O_1 and O_2 exhibits highest negative charge and C_{12} exhibits a maximal positive charge (0.76197, 0.77383, 0.77365, 0.77401 e) for gas, DMSO, methanol and water compared with adjacent elements. A partially positive charge is produced by the C atom and a partial negative charge is developed by the atom of oxygen in a carboxylic acid group. The atom of carbon acquires strongly charged when deprotonation occurs in the acid group, resulting in the carboxylate anion. Carboxylate anion's atom O_1 has a maximum negative charge of -0.70844, -0.6958, -0.6907, -0.69555 e, for

gas, DMSO, methanol and water and it exchanges with the indole ring's nitrogen through intermolecular interactions wherein nitrogen N3 also have highest negative charge -0.5264, -0.52138, -0.5215 and -0.5217 e for gas DMSO, methanol and water. Nitrogen and oxygen are electronegative atoms and are thus attracted to each other electrostatically and hence nearby atom has combination of positive and negative charge C_4 (0.17396, 0.1772, 0.1723 and 0.1722e), C_5 (-0.10534, -0.1127, -0.1126 and -0.1129 e), C_6(0.03701, 0.03418, 0.03419 and 0.03417), C_7 (-0.1937, -0.02039, -0.2036 and -020417 e), C_8 (-0.23495, -0.23577, -0.23579 and -0.23576e), C_{10} (-0.18989, -0.199, -0.1988 and -0.199), C_{11} (-0.22456, -0.23384, -0.23368 and -0.234 e). Atom C_5 has the lowest known negative electrical charge C_5 (-0.10534, -0.1127, -0.1126 and -0.1129 e), wherein adjacent atoms are nitrogen and oxygen and hence becomes negative charge.

ELF and LOL investigation

ELF was initial utilized as a technique to assess atom localization in atomic particles and molecules. This method has been frequently used to investigate atomic along with solid-state chemical bonding [40]. The ELF dumps were gathered with the free Multiwfn 3.8 [15] program. ELF frequencies (shown in red), and electron depleted regions within the valence & innermost shells are indicated by the blue bands surrounding the nuclei. The tone indications for ELF images alternate from blue and red colors ranging from 0.0 to 1.0 and 0.8 to 1.0. The 0.5-1.0 spans show the distribution of the electron domain as well as without connections, yet the 0.5 range shows the de-localized electronic ensemble. The hue shifts from yellow to green for intermediate ELF values of 0.7, blue for lesser ends, and red for high ELF values of 1.4-1.0. The region containing similar electrons in close proximity to N and C was colored blue. Electron pair density is considered in ELF analysis, which provides an electron pair maps with the reference electron's spatial localization. Pauli repulsions, whose values vary from 0 to 1, serve as the foundation for measuring delocalization in an ELF diagram. Electrons were well-localized in the area of highest Pauli repulsion, which is represented by a value of 1, while electrons were delocalized in the region of least Pauli repulsion, which is represented by a value of 0. Significant Pauli repulsion is responsible for the unique electron localization noticed among H-atoms (H13, H14, and H_{20}). The blue areas enclosing all of the carbon atoms (N_3, C_4, C_6, C_5, and C_{12}) show an appearance of scattered electron clouds. Owing to the double binding properties of C-C and C-N bonds, which result in ions containing nitrogen or carbon being classified as blue due to tightly distributed electrons, these blue zones are described. This indicates a high degree of localization. Red highlights depleted covalent electrons in the ring's covalent-sections, which involve carbon and nitrogen atoms. Figure obviously demonstrates that both the gas and solvent parts substantially identical, indicating a successful result. ID2CA is not significantly altered by solvent effects.

IRI and RDG study

Inter-atomic relationships are common in molecular structures. It is particularly effective in the investigation of diverse structural topologies and biological processes because it may detect weaker places for interaction in compounds. IRI is determined by the intensity of the electron and is often utilized to establish chemical connections in macromolecules [41]. Figure S7shows an area with a high density of electrons that improves atom contact, whereas green (feeble-connection zone) and red iso-surfaces indicate influence of steric/repulsive forces. Red flashes in the exact center of this ring in the isosurface suggest steric disdain. Blue color patches indicate stronger positive relationships, such as the strong hydrogen bonds (N_3-H_{13}···O_1 and C_7-H_{14}···O_2). The covalently bonded regions are delineated by the blue surfaces, which exhibit prominent bonding effects and substantial electron density in these locations.

In addition to the current IRI technique, the famous topology strategy known as reduced density gradient technique provides techniques for finding and visualising interactions that are

NCI. It can be used to study and illustrate a variety of noncovalent connections, including interactions caused by vdW, steric conflicts, and hydrogen bonds [42]. Electron intensity and its associated derivatives are analysed to identify noncovalent associations and to determine the exact locations in which such interactions take place. The graphical representation of these interactions is made possible by this study. Plotting ρ(r) versus the sign of λ2ρ provides important information about the nature and vitality of these relationships. In the NCI graphs, the blue zone signified strong hydrogen bonding, but the van der Waals force and steric Configuration NCI analysis is a highly useful approach for estimating the configuration's main physiochemical properties, as non-covalent interactions are important in biological molecules and their interactions with medicinal compounds. A drug's properties, including its capacity to form hydrogen bonds with proteins, can be identified, as can the kind of molecule-solvent interaction that directly alters a molecule's properties. Steric disgust is indicated by red sparks in the very centre of the indolin ring in the RDG isosurface in Figure 5. Red surges are visible in the RDG scattering graphamid 0.010 to 0.05 a.u., which further illustrates the repellent effect. More powerful favourable interactions, namely the strong hydrogen bonds (N_3-H_{13}···O1 and C_7-H_{14}···O_2), are shown by blue colour patches are visible RDG gradient plot. The RDG picture similarly shows such significant associations in a negative range of -0.025 to -0.05 a.u. Furthermore, reddish mixed green areas that are flaky indicate the presence of weak non-covalent interactions N_3-H_{13}···O_1. The above-mentioned interactions are also visible in the 0.01 to -0.02 a.u. region of the RDG map. Figure S8 obviously demonstrates that both the gas & solvent parts substantially identical, indicating a successful result. ID2CA molecule is not significantly altered by solvent effects.

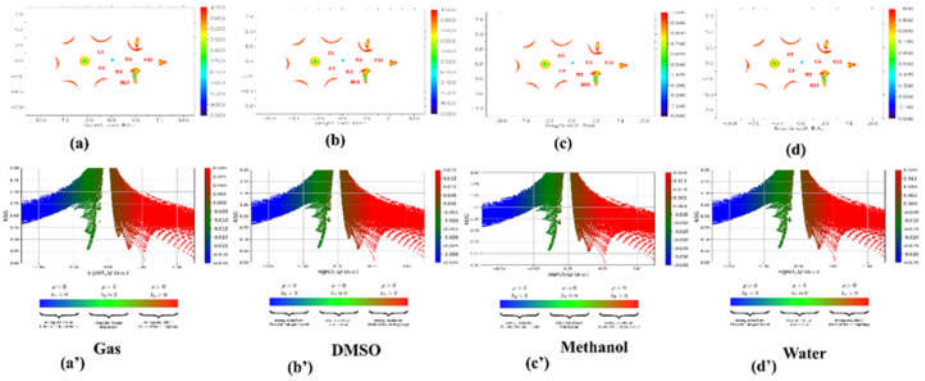

Figure 5: Gradient and RDG scatter plot for ID2CA with different phases.

Pharmaceutical analysis

Drug likeness. Using Lipinski's rule of five [43], counting of drug similarities is an effective method for revealing an active substance. As per this regulation, a ligand is classified as a pharmaceutical medication if it meets specific requirements, such as having a molecular weight of not as much of than 500 Dalton, having an H-bond acceptor count of below 10, having an H-bond donor count of less than 5, and having lipophilicity expressed as log P less than 5. These restrictions completely invalidate the drug similarity testing values presented in Table 3. As a result, it was discovered that there are 2 HBD and 1 HBA for ID2CA molecule. The values that were observed for log P were 1.86, indicating a lipophilic characteristic for the title compound.

Table 3. Drug likeness descriptors of ID2CA.

Descriptors	Calculated
Molecular mass (Dalton)	161.16
Hydrogen bond donor	2
Hydrogen bond acceptor	1
Log P	1.8661
Number of rotatable bonds	1
Topological polar surface area (TPSA) ($Å^2$)	68.643

Ramachandran plot

For docking studies, the protein molecule was chosen for study using the Ramachandran (RC) graph as a stability indicator. Superoxide dismutase (SOD) was anticipated through the PASS online [44] predictor, and the results are shown in Table S8. The enzyme known as SOD is responsible for catalyzing the conversion of superoxide radicals into regular molecules of O and H-peroxide. Superoxide is a by-product of O metabolism that, if not controlled, may lead to a variability of cell injuries [45]. Hydrogen peroxide, another harmful chemical, is broken down by enzymes like catalase. Consequently, in almost all living cells that are exposed to oxygen, Superoxide dismutase (SOD) functions as a vital antioxidant defence system. Through structural alignment in RC plots, target proteins were suitably chosen and verified for docking applications. For the proteins (4B3E, 2C9V, 1SOS, and 1DO5) a sizable percentage of amino acids (89.3%, 93.4%, 86.8%, and 84.2%, accordingly) are within the allowable range. The low frequency of amino acids in the confined area indicates structural stability of proteins picked for contact. These illustrations show that the chosen receptors (PDB IDs: 4B3E, 2C9V, 1SOS, and 1DO5) show structural stability, which qualifies them as viable options for docking onto the ID2CA molecule.

Molecular docking analysis

Molecular docking is important in the field of medicine because it provides significant information on how a ligand interacts with its target protein [46]. This area of bioinformatics determines the precise amino acid residues that the ligand binds to attach to the protein's site of action. It also determines the kinds and distances of bonds that form among the ligand and the amino acids. This approach is critical to the discovery of novel medications since it establishes if a ligand under study will interact biologically with the desired receptor protein. The particularity of a ligand for a given targeted protein is critical in drug-receptor contact and therapeutic development [47]. Identifying ligands that are unique to their desired target proteins is made easier with the help of molecular docking. Ligands that don't interact biologically with a specific protein aren't considered good candidates for additional research. The relationships between an ID2CA molecule and several antioxidant proteins were evaluated in the study using molecular docking. The 2D and 3D visual representations of the relationship amid the investigated ligand and receptor protein are provided in Figure. 6, while the outcomes, shown in Table S9, showed the binding ability of ID2CA with multiple proteins (4B3E, 2C9V, 1SOS, and 1DO5). Based on computations, the binding energies of proteins (4B3E, 2C9V, 1SOS, and 1DO5) are -4.93, -7.07, -4.72 and -4.05 kcal/mol, and their matching inhibition constants of 245.08 μM, 6.61 μM, 349.18 μM, and 1.07 mM, are ascertained. Protein 2C9V had the lowest binding interaction value (-7.07 kcal/mol) and inhibition constant (6.61 μM) among all targets. The interaction between the ligand and contributor residues (amino acids) in the ID2CA molecule, such as LYS 30 and GLU 100, involves H_{19} and O_2 atoms and has bond radii of 1.56, 3.00 Å, and 2.16 Å. Given its higher binding energy arrangement, the docking study suggests that ID2CA has a significant pharmacological effect as an inhibitor of antioxidants.

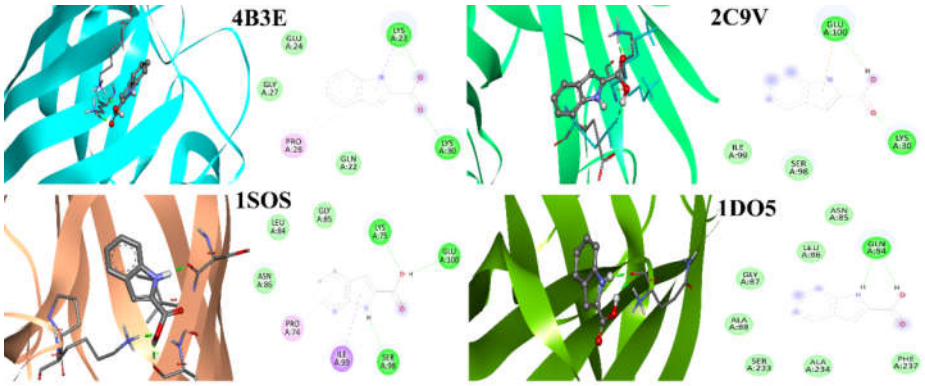

Figure 6. 3D and 2D interactions of molecular docking with antioxidant proteins.

Molecular dynamic (MD) simulation

MD simulations are widely employed in drug development to assess protein-ligand (PL) stability. It is possible to examine the continuity and intensity of the PL connection by tracking the movement of ligand and protein in a physiologically realistic setting. Moreover, all-atom 100 ns MD calculations were achieved on ligand (ID2CA)-2C9V (protein) docked complex, which had the highest binding affinity. "Protein topology was generated using the CHARMM27 force field. The ligand topology and data suitable with GROMACS were generated using the Swiss Param Server" [48]. The entire system was dissolved utilizing the TIP3P water model following neutralization with the appropriate amounts of Na^+ and Cl^- ions. The system conducted ensemble equilibration at 1 ns NVT and 1 ns NPT. After correcting for PBC and excluding solvents, ions, and other particles from the 100 ns atomistic MD trajectory, embedded functions of GROMACS 2022 were implemented to calculate the multiple essential variables, including RMSD, RMSF, Rg, and numerous H-bonds between 2C9V and ID2CA.

One important metric to consider when examining the equilibration of MD trajectories is the RMSD, which is computed for the backbone atoms of PL complexes. Using RMSF, average variability of all residues during the simulation was determined. The interactions between ID2CA and 2C9V were uncovered to have an average RMSD of 0.75 nm. Protein (2C9V) varies most, reaching over 0.53 nm. It indicates a reduction in protein stability brought on by ligand binding. Extremely large variations in RMSD and RMSF could indicate protein-ligand complex instability or a significant structural shift that the protein has undergone. The Rg's consistency demonstrated the protein's stability.

Calculating "binding free energy (ΔG binding) of protein-ligand complexes" was made possible by applying MMPBSA to the MD trajectory [49]. The MMPBSA was derived from the whole 100 ns trajectory by obtaining snapshots of the MD model at 10-frame spacing (0.1 ns). Protein-ligand complexes' ΔG binding quantifies their interactions. "The protein-ligand binding energy was determined utilizing a particular equation: G complex - (G receptor + G ligand) = ΔG binding, where ΔG binding is the complex's total binding energy, G receptor is its free receptor's binding energy, and G ligand is its unbounded ligand's energy". Another approach to express G binding is as "ΔG binding = ΔH –TΔS, where ΔH is binding enthalpy and -TΔS is the entropy component following ligand binding. The gauged value is referred to as the effective free energy if the entropic term is ignored. This value is typically sufficient for evaluating comparative binding free energies for alike systems. From Table 4, ID2CA molecule found that the average effective free energy of binding is 5.87 ± 2.03 kcal/mol.

Table 4. Free energy of binding obtained using MMPBSA calculations (considering all frames from 100 ns).

Delta (complex - receptor - ligand)		
Energy component	Average (kcal/mol)	Standard deviation
ΔBOND	0	0
ΔANGLE	0	0
ΔDIHED	0	0
ΔUB	0	0
ΔIMP	0	0
ΔCMAP	0	0
ΔVDWAALS	-6.05	1.25
ΔEEL	-5.05	6.73
Δ1-4 VDW	0	0
Δ1-4 E_{EL}	0	0
ΔE_{PB}	13.88	5.39
ΔEN_{POLAR}	-5.65	0.70
ΔE_{DISPER}	9.75	0.90
ΔG_{GAS}	-12.10	7.02
ΔG_{SOLV}	17.98	5.35
ΔTOTAL	5.87	2.03

CONCLUSION

Under DFT optimization, the ID2CA molecule was shown to have characteristics in the gas phase that closely resembled the stated experimental XRD findings for both gas and polar solvents (DMSO, methanol, and water). The vibrational spectra are thoroughly interpreted with the aid of NCA analysis. FT-IR spectra have recorded and the values agreed with the theoretical vibrational assortments. Through the use of RDG visualization and ELF color charts, which emphasize electrophilic sites (mostly the aromatic hydrogens) & nucleophilic locations (N_3, C_4, C_6, C_5, and C_{12}), wavefunction investigations shed information on the bonding zones inside the molecule. Reduced band gap values were revealed by the estimated HOMO-LUMO gaps in the gas and solvent phases, which are 4.418 eV (gas), 4.362 eV (DMSO), 4.368 eV (methanol), and 4.300 eV (water). This might account for the ID2CA compound's bioactivity. The TD-DFT approach yielded UV λ_{max} values of 287.63 nm for water, 287.54 nm for methanol, and 289.14 nm for DMSO. These values corresponded to the measured peaks at 293 nm for DMSO and 292 nm for methanol. The sites that reacted were identified using MEP analysis, which included nucleophilic nitrogen, hydroxyl atoms, and electrophilic oxygen. NBO study confirmed stabilization inside the molecule. Additionally, pharmacological assessments were performed to ascertain the compound's drug-likeness & toxicity; the outcomes suggested the compound's strong medical application. Molecular docking towards antioxidant targets (4B3E, 2C9V, 1SOS, and 1DO5) revealed reduced (negative) binding affinities of -4.93, -7.07, -4.72, and -4.05 kcal/mol, respectively, showing the possibility for antioxidant properties. Also the Ramachandran plot is potted for the targeted proteins. As a result of findings, the compound is a viable therapeutic candidate.

ACKNOWLEDGEMENTS

We acknowledge Dayalbagh Educational Institute, Agra and Jamia Millia Islamia, New Delhi, for research facility.

FUNDING

This research project was supported by Researchers Supporting Project number (RSPD2024R1116), King Saud University, Riyadh, Saudi Arabia.

REFERENCES

1. Sravanthi, T.V.; Manju, S.L. Indoles - a promising scaffold for drug development. *Eur. J. Pharm. Sci.* **2016**, 91, 1-10.
2. Lakhdar, S.; Westermaier, M.; Terrier, F.; Goumont, R.; Boubaker, T.; Ofial, A.R.; Mayr, H. Nucleophilic reactivities of indoles. *J. Org. Chem.* **2006**, 71, 9088-9095.
3. Barluenga, J.; Valdés, C. *Five-Membered Heterocycles: Indole and Related Systems* in *Modern Heterocyclic Chemistry* , Wiley: Online Library; **2011**.
4. Kaushik, N.K.; Kaushik, N.; Attri, P.; Kumar, N.; Kim, C.H.; Verma, A.K.; Choi, E.H. Biomedical importance of indoles. *Molecules* **2013**, 18, 6620-6662.
5. Huang, N.Y.; Liu, M.G.; Ding, M.W. Efficient regioselective synthesis of indole n-carboximidamides and n-carboximidoates by a sequential aza-wittig/Ag(I)-catalyzed cyclization. *J. Org. Chem.* **2009**, 74, 6874-6877.
6. Kalaskar, G.P.; Girisha, M.; Purohit, M.G.; Thippeswamy, B.S.; Pati, B.M. Synthesis and evaluation of in vivo antiinflammatory activity of indole-3-acetic acids. *Indian J. Heterocycl. Chem.* **2007**, 16, 325-328.
7. Rani, P.; Srivastava, V.K.; Kumar, A. Synthesis and antiinflammatory activity of heterocyclic indole derivatives. *Eur. J. Med. Chem.* **2004**, 39, 449-452.
8. Meenakumari, V.; Mangaiyarkkarasi, J.; Premkumar, R.; Asath, R.M.; Benial, A.M.F.; Thenmozhi, N. Spectroscopic characterization, quantum chemical and molecular docking investigations on methyl indole-3-carboxylate: A potent cervical cancer drug. *J. Mol. Struct.* **2024**, 1305, 137711.
9. El-Lateef, H.M.A.; Khalaf, M.M.; Abdou, A. Preparation, characterization, in vitro biological evaluation, DFT calculations, and molecular docking investigations of 1H-imidazole-2-carboxylic acid and histidine-based mixed-ligand complexes. *Chem. Biodivers.* **2024**, e202402049.
10. Frisch, M.J.; Trucks, G.W.; Schlegel, H.B.; Scuseria, G.E.; Robb, M.A.; Cheeseman, J.R.; Scalmani, G.; Barone, V.; Petersson, G.A.; Nakatsuji, H.; Li, X.; Caricato, M.; Marenich, A.V.; Bloino, J.; Janesko, B.G.; Gomperts, R.; Mennucci, B.; Hratchian, H.P.; Ortiz, J.V.; Izmaylov, A.F.; Sonnenberg, J.L.; Williams-Young, D.; Ding, F.; Lipparini, F.; Egidi, F.; Goings, J.; Peng, B.; Petrone, A.; Henderson, T.; Ranasinghe, D.; Zakrzewski, V.G.; Gao, J.; Rega, N.; Zheng, G.; Liang, W.; Hada, M.; Ehara, M.; Toyota, K.; Fukuda, R.; Hasegawa, J.; Ishida, M.; Nakajima, T.; Honda, Y.; Kitao, O.; Nakai, H.; Vreven, T.; Throssell, K.; Montgomery Jr., J.A.; Peralta, J.E.; Ogliaro, F.; Bearpark, M.J.; Heyd, J.J.; Brothers, E.N.; Kudin, K.N.; Staroverov, V.N.; Keith, T.A.; Kobayashi, R.; Normand, J.; Raghavachari, K.; Rendell, A.P.; Burant, J.C.; Iyengar, S.S.; Tomasi, J.; Cossi, M.; Millam, J.M.; Klene, M.; Adamo, C.; Cammi, R.; Ochterski, J.W.; Martin, R.L.; Morokuma, K.; Farkas, O.; Foresman, J.B.; Fox, D.J. Gaussian, Inc., Wallingford CT (2016) GaussView 5.0. Wallingford, E.U.A. Gaussian 16, Revision C. 01. **2016**.
11. Divya, P.; Jeba Reeda, V.S.; Suja, R.; Bena Jothy, V. Structural activity, spectroscopic, fukui, NCI, AIM, IGM combined with molecular docking and molecular dynamics simulation on 4-methylpyridinium 4-hydroxybenzoate-potent drug anti-leukemia cancer. spectrochim. *Acta - Part A Mol. Biomol. Spectrosc.* **2024**, 306, 123568.
12. Sundius, T. Molvib - a flexible program for force field calculations. *J. Mol. Struct.* **1990**, 218, 321-326.
13. Boyle, N.M.O'; Tenderholt, A.L.; Langner, K.M. Software news and updates cclib: a library for package-independent computational chemistry algorithms. *J. Comput. Chem.* **2008**, 29, 839-845.
14. M.J. Dennington RD, T.A.K. Gauss View5.0.8, Gaussian Inc; Wallingford; **2016**.
15. Lu, T.; Chen, F. Multiwfn: A multifunctional wavefunction analyzer. *J. Comput. Chem.* **2012**, 33, 580-592.

16. Humphrey, W.; Dalke, A.; Schulten, K. VMD: visual molecular dynamics. *J. Mol. Graph.* **1996**, 14, 33-38.
17. Daina, A.; Michielin, O.; Zoete, V. SwissADME: A free web tool to evaluate pharmacokinetics, drug-likeness and medicinal chemistry friendliness of small molecules. *Sci. Rep.* **2017**, 7, 1-13.
18. Morris, G.M.; Huey, R.; Olson, A.J. Using AutoDock for ligand-receptor docking; **2008**.
19. Biovia, D.S. Discovery Studio Modeling Environment; release 4.5. Dassault Systèmes BIOVIA, San Diego, 4; **2015**.
20. Abraham, M.J.; Murtola, T.; Schulz, R.; Páll, S.; Smith, J.C.; Hess, B.; Lindah, E. GROMACS: High performance molecular simulations through multi-level parallelism from laptops to supercomputers. *SoftwareX* **2015**, 1-2, 19-25.
21. Scott, W.R.P.; Hünenberger, P.H.; Tironi, I.G.; Mark, A.E.; Billeter, S.R.; Fennen, J.; Torda, A.E.; Huber, T.; Krüger, P.; Van Gunsteren, W.F. The GROMOS biomolecular simulation program package. *J. Phys. Chem. A.* **1999**, 103, 3596-3607.
22. Zoete, V.; Cuendet, M.A.; Grosdidier, A.; Michielin, O. SwissParam: A fast force field generation tool for small organic molecules. *J. Comput. Chem.* **2011**, 32, 2359-2368.
23. Morzyk-Ociepa, B.; Michalska, D.; Pietraszko, A. Structures and vibrational spectra of indole carboxylic acids. Part I. Indole-2-carboxylic acid. *J. Mol. Struct.* **2004**, 688, 79-86.
24. Divya, P.; Jeba Reeda, V.S.; Jothy, V.B. Spectroscopic investigations and electronic transitions, topology studies, and biological assay of a potent antimicrobial compound: 2-amino-pyrimidine benzoic acid. *Spectrosc. Lett.* **2023**, 0, 1-16.
25. Eşme, A.; Sağdınç, S.G. Spectroscopic (FT–IR, FT–Raman, UV–Vis) analysis, conformational, HOMO-LUMO, NBO and NLO calculations on monomeric and dimeric structures of 4–pyridazinecarboxylic acid by HF and DFT methods. *J. Mol. Struct.* **2017**, 1147, 322-334.
26. Kanimozhi, R.; Arjunan, V.; Mohan, S. Conformations, structure, vibrations, chemical shift and reactivity properties of isoquinoline–1–carboxylic acid and isoquinoline–3–carboxylic acid – comparative investigations by experimental and theoretical techniques. *J. Mol. Struct.* **2020**, 1207, 127841.
27. Socrates, G. *Infrared and Raman Characteristic Group Frequencies*, Wiley: New York; **2001**.
28. Saravanan, S.; Balachandran, V. Quantum mechanical study and spectroscopic (FT-IR, FT-Raman, UV-Visible) study, potential energy surface scan, fukui function analysis and HOMO-LUMO analysis of 3-tert-butyl-4-methoxyphenol by DFT methods. *Spectrochim. Acta - Part A Mol. Biomol. Spectrosc.* **2014**, 130, 604-620.
29. Arulraj, R.; Sivakumar, S.; Suresh, S.; Anitha, K. Synthesis, vibrational spectra, DFT calculations, hirshfeld surface analysis and molecular docking study of 3-chloro-3-methyl-2,6- diphenylpiperidin-4-one. Spectrochim. *Acta Part A Mol. Biomol. Spectrosc.* **2020**, 232, 118166.
30. Vasantha Kumar, V.; Goud, S.L.; Laxmikanth Rao, J. Ab initio and density functional theory studies on vibrational spectra of 3-hydroxy-3-(2-methyl-1h-indol-3-yl)indolin-2-one. *Spectrochim. Acta - Part A Mol. Biomol. Spectrosc.* **2013**, 103, 304-310.
31. Subramanian, N.; Sundaraganesan, N.; Jayabharathi, J. Molecular structure, spectroscopic (FT-IR, FT-Raman, NMR, UV) studies and first-order molecular hyperpolarizabilities of 1,2-bis(3-methoxy-4-hydroxybenzylidene)hydrazine by density functional method. *Spectrochim. Acta - Part A Mol. Biomol. Spectrosc.* **2010**, 76, 259-269.
32. Jeba Reeda, V.S.; Bena Jothy, V.; Asif, M.; Nasibullah, M.; Alharbi, N.S.; Abbas, G.; Muthu, S. Synthesis, solvent polarity(polar and nonpolar), structural and electronic properties with diverse solvents and biological studies of (e)-3-((3-chloro-4-fluorophenyl) imino) indolin-2-one. *J. Mol. Liq.* **2023**, 380, 121709.
33. Ramesh, P.; Gunasekaran, S.; Ramkumar, G.R. Molecular structure, vibrational spectra, UV - visible a Nd NMR spectral analys is on ranitidine hydrochloride u sing ab initio a Nd DFT methods. *Int. J. Curr. Res. Acad. Rev.* **2015**, 3, 117-138.

34. Muthu, S.; Elamurugu Porchelvi, E.; Karabacak, M.; Asiri, A.M.; Swathi, S.S. Synthesis, structure, spectroscopic studies (FT-IR, FT-Raman and UV), normal coordinate, NBO and NLO analysis of salicylaldehyde p-chlorophenylthiosemicarbazone. *J. Mol. Struct.* **2015**, 1081, 400-412.
35. Akman, F.; Demirpolat, A.; Kazachenko, A.S.; Kazachenko, A.S.; Issaoui, N.; Al-Dossary, O. Molecular structure, electronic properties, reactivity (ELF, LOL, and Fukui), and NCI-RDG studies of the binary mixture of water and essential oil of *Phlomis bruguieri*. *Molecules* **2023**, 28, 2684.
36. Reeda, V.S.J.; Jothy, V.B.; Asif, M.; Nasibullah, M.; Kadaikunnan, S.; Abbas, G.; Muthu, S. Synthesis, functional group analysis (experimental and theoretical), solvent – solute interactions, structural insights of (e)-3-(4-chloro-3-(trifluoromethyl) phenyl) imino) indolin-2-one–in-vitro antimicrobial activity. *J. Mol. Struct.* **2023**, 1294, 136310.
37. Reeda, V.J.; Sakthivel, S.; Divya, P.; Javed, S.; Jothy, V.B. Conformational stability, quantum computational (DFT), vibrational, electronic and non-covalent interactions (QTAIM, RDG and IGM) of antibacterial compound n-(1-naphthyl)ethylenediamine dihydrochloride. *J. Mol. Struct.* **2024**, 1298, 137043.
38. Ayers, P.W.; Parr, R. Variational principles for describing chemical reactions: The fukui function and chemical hardness revisited. *J. Am. Chem. Soc.* **2000**, 122, 2010-2018.
39. Morell, C.; Grand, A.; Toro-Labbé, A. New dual descriptor for chemical reactivity. *J. Phys. Chem. A*. **2005**, 109, 205-212.
40. Irfan, A.; Hussien, M.; Chaudhry, A.R.; Qayyum, M.A.; Al-Sehemi, A.G.; Selvakumari, S.; Muthu, S. Effect of solvent role in electronic properties, band gap, electron injection barrier, charge transport nature, topology studies (ELF, LOL, RDG), and optical properties of azoles for multifunctional applications. *J. Mol. Liq.* **2023**, 390, 122956.
41. Sravanthi, R.; Mahalakshmi, S.; Vetrivelan, V.; Irfan, A.; Muthu, S. Absorption wavelength (TD-DFT) and adsorption of metal chalcogen clusters with methyl nicotinate: Structural, electronic, IRI, SERS, pharmacological and antiviral studies (HIV and Omicron). *Heliyon.* **2023**, 9, e16066.
42. Rayene, K.; Imane, D.; Abdelaziz, B.; Leila, N.; Fatiha, M.; Abdelkrim, G.; Bouzid, G.; Ismahan, L.; Brahim, H.; Rabah, O. Molecular modeling study of structures, hirschfield surface, NBO, AIM, RDG, IGM and ^{1}HNMR of thymoquinone/hydroxypropyl-β-cyclodextrin inclusion complex from QM calculations. *J. Mol. Struct.* **2022**, 1249, 131565.
43. Lipinski, C.A. Lead- and drug-like compounds: The rule-of-five revolution. *Drug Discov. Today Technol.* **2004**, 1, 337-341.
44. Lagunin, A.; Stepanchikova, A.; Filimonov, D.; Poroikov, V. PASS: Prediction of activity spectra for biologically active substances. *Bioinformatics* **2000**, 16, 747-748.
45. Hayyan, M.; Hashim, M.A.; Alnashef, I.M. Superoxide ion: Generation and chemical implications. *Chem. Rev.* **2016**, 116, 3029-3085.
46. Meng, X.-Y.; Zhang, H.-X.; Mezei, M.; Cui, M. Molecular docking: A powerful approach for structure-based drug discovery. *Curr. Comput. Aided-Drug Des.* **2012**, 7, 146-157.
47. Jeba Reeda, V.S.; Divya, P.; Suja, R.; Rathika, A.; Bena Jothy, V. Synthesis, spectroscopic investigations, topological non-covalent interactions, chemical reactivity, molecular docking and molecular dynamic simulation on piperazine succinate - a potential antimicrobial compound. *J. Mol. Struct.* **2023**, 1292, 136179.
48. Singh, P.; Sharma, P.; Bisetty, K.; Perez, J.J. Molecular dynamics simulations of Ac-3Aib-Cage-3Aib-NHMe. *Mol. Simul*. **2010**, 36, 1035-1044.
49. Kumari, R.; Kumar, R.; Lynn, A. G-Mmpbsa -A GROMACS tool for high-throughput MM-PBSA calculations. *J. Chem. Inf. Model.* **2014**, 54, 1951-1962.